ACS Photonics

pubs.acs.org/journal/apchd5

Article

Photonic Orbital Angular Momentum Dichroism on Three-Dimensional Chiral Oligomers

Yang Cao, Shunli Liu, Yuan Tao, Xinghao Wang, Jincheng Ni, Chaowei Wang, Xinyuan Zheng, Jiawen Li,* Yanlei Hu, Dong Wu, and Jiaru Chu

Cite This: *ACS Photonics* 2023, 10, 1873–1881

Read Online

ACCESS | Metrics & More | Article Recommendations | Supporting Information

ABSTRACT: Chiral oligomers in optics are photonic metamaterials inspired by the concept of chiral centers in chemistry. In recent years, chiral oligomers have attracted increasing attention in recent years due to their simple construction and unique chiroptical response. To date, research has predominantly focused on the photonic spin angular momentum (SAM)-dependent chiroptical response: circular dichroism (CD). However, for another photonic dimension parallel to the SAM, orbital angular momentum (OAM)-dominated chiroptical response of chiral oligomers still remains elusive. Here, we theoretically and experimentally demonstrate the individual three-dimensional (3D) chiral tetramers can exhibit a gigantic response to the photonic OAM with a maximum helical dichroism (HD) of ~23%. Meanwhile, we also reveal the origin of the HD via simulation analysis of electric current distribution, reflected electric field, and the discrete OAM spectroscopy. Furthermore, by femtosecond direct laser writing, 3D oligomers with tailoring geometric parameters can be flexibly fabricated in one step for varying HD responses. Our research fills the gap of OAM-related chiroptical response of chiral oligomers, which has great implications for chiroptical spectroscopy and photonic angular momentum engineering.

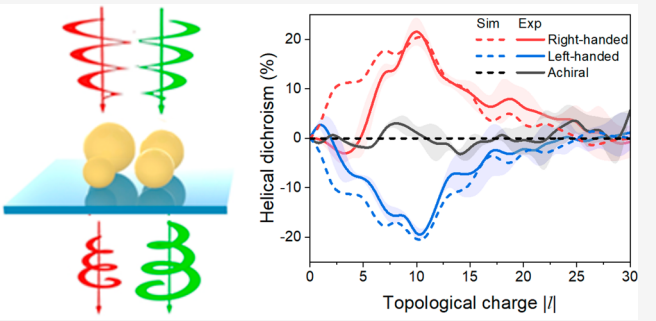

KEYWORDS: *chiral oligomers, chiral center, optical vortex, orbital angular momentum, helical dichroism*

INTRODUCTION

Chirality is the basic property of the material world, which is reflected in the birth and evolution of life.[1−3] A mass of biomolecules in living organisms are chiral, e.g., carbohydrates,[4] essential amino acids,[5] and nucleic acids.[6] Among these chiral biomolecules, the common feature is the so-called chiral center, which is a tetrahedral atom (generally a tetravalent carbon atom) connected with four different atoms or molecular groups.[7,8] Chiral center is an archetype chiral system with simple configurations and interesting characteristics, whose handedness is determined by the order in which the atoms are arranged. In recent years, researchers have been keen to transfer a famous and promising concept to the realm of optical metamaterials by drawing inspiration from chemistry, as well as molecular and atomic physics.[9−12] In this context, chiral oligomers, one of the most flexible optical metamaterials, have been introduced to construct the analogues of chiral centers.[13,14] These artificial chiral oligomers are nanoantenna ensembles composed of several ligands with varying parameters, which can be prepared by electron beam lithography,[15] colloidal lithography,[16] direct laser writing (DLW), etc.[17]

Over the past decade, the chiroptical response of these artificial chiral oligomers has attracted widespread attention. In 2009, the optical activity of mixed pyramidal oligomers was first observed by A. J. Mastroianni et al.[18] Afterward, M. Hentschel et al. demonstrated that chiral oligomers, similar to molecular systems, enable encoding of their three-dimensional arrangement to achieve unique and well-modulated spectra.[19] Recently, P. Banzer et al. designed a set of trimers composed of heterogeneous materials to make their optical response highly tunable, further improving the design freedom of the chiral oligomers.[20] However, all of this research consistently focused on the photonic spin angular momentum (SAM)-dependent circular dichroism (CD), while chiroptical response of another vital photonic dimension, orbital angular momentum (OAM), is ignored and not investigated.

Generally, the photonic OAM characterized by a helical phase wavefront is inherently carried by chiral optical vortices, which is essentially different from the SAM carried by circularly polarized light.[21−24] As an emerging photonic

Received: February 27, 2023
Published: June 7, 2023

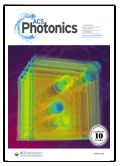

https://doi.org/10.1021/acsphotonics.3c00266
ACS Photonics 2023, 10, 1873−1881

dimension, the OAM has been widely applied in metasurface,[25,26] optical communications,[27] super-resolution fluorescence microscopy,[28,29] optical tweezers,[30] and micro/nanomanufacturing,[31,32] also showing great potential in the field of light−matter interaction.[33] Especially, the OAM has been used for probing the chirality of microscopic objects by a novel chiroptical response, referred to as helical dichroism (HD) to distinguish it from the SAM-dependent CD.[34−36] In 2018, Kerber et al.[37,38] considered the interaction of optical vortices with a metallic Archimedean spiral structure and observed HD phenomenon. Fang et al.[39] then used chiral metal nanoparticles to observe different spectra at different momenta. Recently, the viability of nanoscale information multiplexing utilizing HD is demonstrated.[40−42] According to recent advances, the concept of detecting the chirality of molecules by HD has been validated as well.[43,44] Therefore, as analogs of chiral molecules, it is of great significance to explore the helical dichroism of artificial chiral oligomers in the OAM dimension.

Herein, we first demonstrated the concept of helical dichroism of an individual 3D chiral oligomer in the photonic OAM dimension. The 3D chiral tetramer, consisting of four microspheres with different diameters arranged according to the preset chirality, allowing the selective transmission of incident optical vortices with opposite topological charges ($+l$, $-l$). By measuring and analyzing the topological charge reflectance spectra of left- and right-handed 3D tetramers, mirror-symmetric HD spectra with a maximum value of ∼23% can be observed in the experiments and simulations. In addition, we also reveal the origin of HD through a variety of simulation analysis, including electric current distribution, electric field distribution, and the discrete OAM spectroscopy. Maximum signal and peak position, the two most important features of the HD spectrum, can be flexibly tailored by adjusting the parameters of oligomers, e.g., the ligands number and separation distance. We believed that the finding of helical dichroism on the 3D chiral oligomers via optical vortices will contribute to advanced chiral spectroscopy and programmable chiral metamaterial design.

RESULTS AND DISCUSSION

Concept of OAM-Dependent HD Measurement Using Optical Vortices. Chiral light waves can carry angular momentum (AM) induced by their polarization and spatial wavefront. As early as 1909, Poynting discovered that circularly polarized light has either left or right circular polarization states depending on the carrying SAM.[45] Similarly, an optical vortex characterized by a helical wavefront also possesses handedness due to the OAM, and its phase distribution can be described as $e^{il\varphi}$, where φ is the azimuthal angle and the integer l is the unbounded topological charge.[46,47] Similar as circular dichroism (CD), helical dichroism (HD) refers to the differential absorption of optical vortices with opposite handedness by chiral molecules or materials that exhibit a helical structure. Note that the phenomenon can be observed in both reflection and transmission experiments. As shown in the schematic diagram in Figure 1b, taking an individual 3D chiral tetramer for example, when the left- and right-handed optical vortices are irradiated on it, their transmitted light intensities show giant asymmetry, which is in sharp contrast to the symmetric transmission in the achiral tetramer (Figure 1a).

It is worth mentioning that, unlike Gaussian beam, the optical vortex with a nonzero topological charge l has a "doughnut-shaped" light intensity profile and helical wavefront,

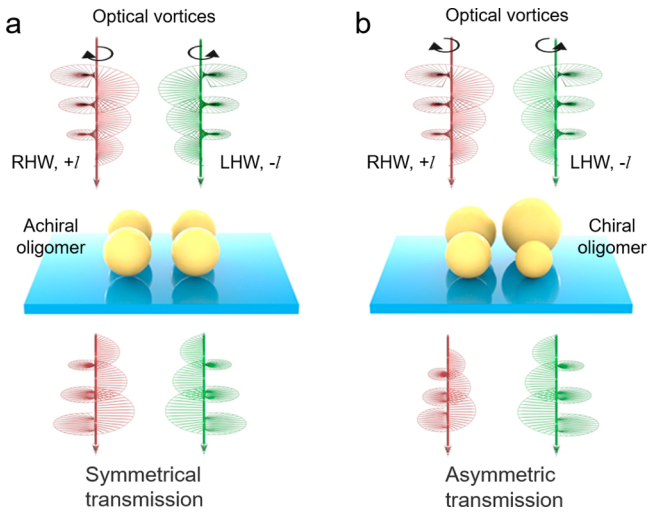

Figure 1. Concept of photonic OAM-dependent HD in 3D oligomers. Illustration of the achiral (a) and left-handed (b) individual tetramers illuminated by opposite optical vortices ($+l$, $-l$) at normal incidence. Unlike achiral one, optical vortices exhibit asymmetric transmission as they pass through the chiral tetramer. This phenomenon is defined as helical dichroism (HD).

as shown in Figure 2a. When $l = -1$, the phase wavefront of the beam is twisted into a helical plane. Due to the Poynting vector is always perpendicular to the wavefront, it is no longer parallel to the optical axis, but follows a helix trajectory. When $l = 1$, the phase wavefront of the optical vortex twists in the opposite direction to $l = -1$. The phase change is $2\pi l$ for each revolution around the optical axis. Meanwhile, with the increase of l value, the distortion degree of the wavefront expands, and the annular diameter of the optical vortex also increases.

The experimental setup for HD measurement of 3D oligomers by optical vortices is illustrated in Figure 2b. The femtosecond laser beam is regulated to linear polarization state by a half-wave plate and a Gran-Taylor prism, and then reflected by a plane mirror M1 and illuminated on a phase-only spatial light modulator (SLM). Optical vortices with tunable topological charge l are generated by loading controllable fork grating holograms on the SLM. The linearly polarized optical vortex is illuminated on the individual oligomers at normal incidence through a 100× objective lens after beam reduction through the 4f lens system L1 and L2, avoiding any chiral disturbance from photonic SAM or extrinsic helicity of light. The doughnut-shaped intensity profiles of high-quality optical vortices can be caught by the charge-coupled device (CCD) camera (Figure 2c). After aligning the center of the individual oligomer and the optical axis of the optical vortex through the nano mobile platform, the distribution of the reflected light is obtained by the CCD and the normalized reflectance was analyzed by a computer.

As shown in Figure 2d, the design of the 3D chiral tetramer is evolved from a combination of chiral molecules and 3D helices, manifesting four microspheres of different diameters arranged in a helix trajectory. Since the central carbon atom has no material effect on the handedness of the chiral center, there is no counterpart of it in our structure, only the four atoms fixed at the corners of the symmetric tetrahedron are represented by four spherical ligands. Similar construction rules have been utilized in earlier work.[9,18,48] The gold-plated

https://doi.org/10.1021/acsphotonics.3c00266
ACS Photonics 2023, 10, 1873−1881

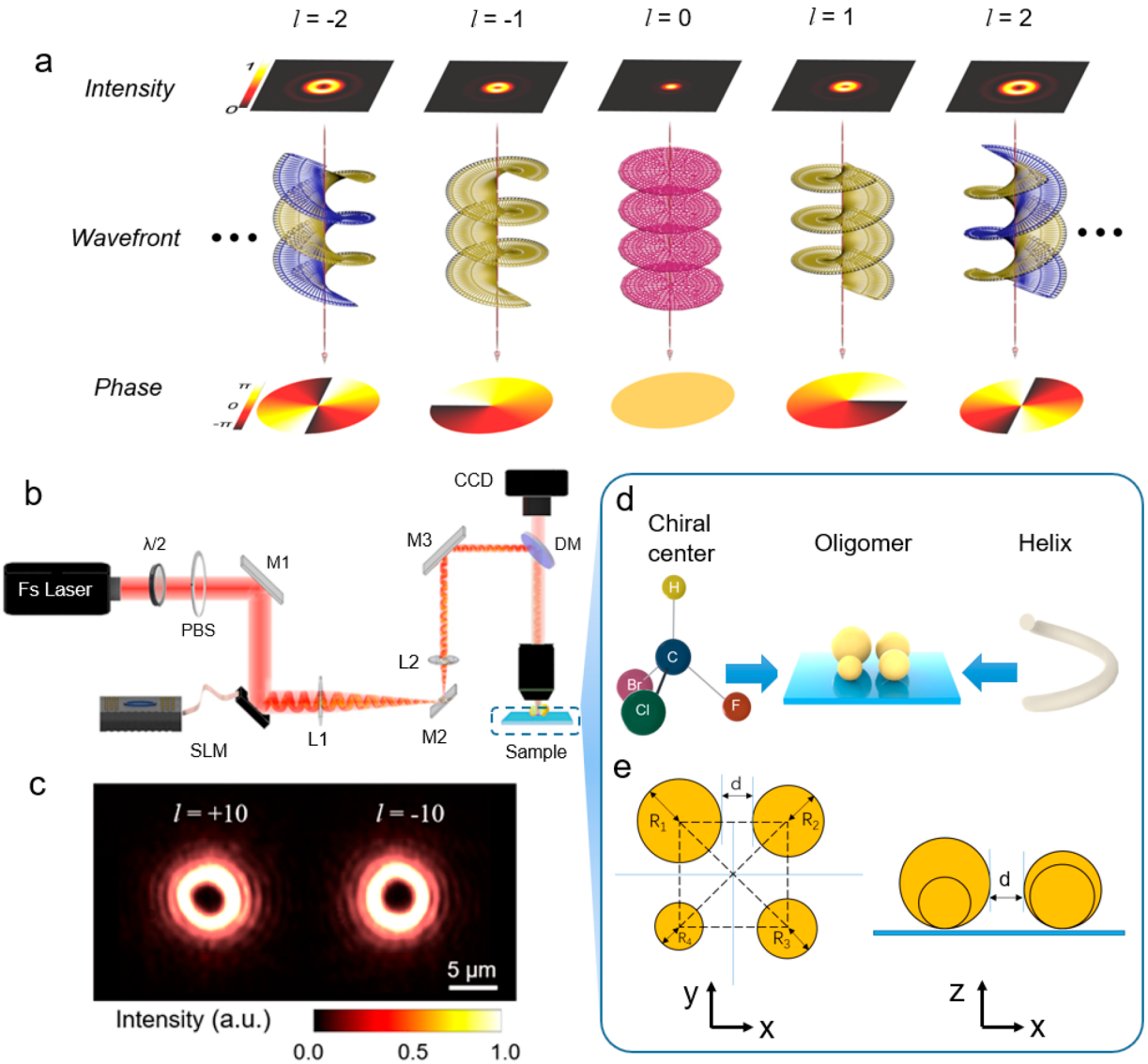

Figure 2. Properties of optical vortices and HD measurement on the individual 3D oligomers. (a) Intensity profile (top), helical wavefront (middle), and phase distributions (bottom) corresponding to the topological charge l of optical vortices. (b) Experimental setup implemented for measuring HD on 3D oligomers. $\lambda/2$, half wave plate; PBS, polarization beam splitter; DM, dichroic mirror. (c) Optical images of optical vortices with topological charges l = +10 and −10. (d) The design of the 3D chiral tetramer is bioinspired from a chiral molecule and reference the structural features of 3D helices. (e) Schematic diagram of top and front views of right-handed tetramers. The minimum distance between the edge of two largest ligands is defined as separation distance d.

3D oligomers is fabricated by femtosecond direct laser writing commercial photoresist SZ2080, and then coated with the ion sputtering coater (see more details in the Methods section). Figure 2e exhibits the vertical and forward views of the individual 3D chiral tetramers, respectively. The spherical ligands are tangent to the silica substrate below, and the mapping of them coordinated on the substrate forms a square. The diameters of spherical ligands are 1600, 2000, 2400, and 2800 nm in ascending order. The minimum distance between the edges of the two largest ligands is defined as the separation distance d. As a control, we also designed the achiral tetramer consisting of four ligands in the same size, each with a diameter of 2200 nm (the average size of the four ligands in chiral tetramers).

Experimental and Simulated Reflectance Spectra and HD Spectra of 3D Oligomers. On account of HD considering the interaction of photonic OAM with chiral oligomers, the reflectance of varying optical vortices at a fixed wavelength (800 nm) is measured, resulting in normalized reflectance spectra with topological charge as an independent variable. In the case of the same incident optical intensity distribution, for right-handed tetramers, the reflection of the right-handed optical vortices ($+l$) is stronger than that of the left-handed ones ($-l$) at topological charge $|l|$ from 2 to 25, as demonstrated in Figure 3a. When the topological charge $|l|$ is greater than 25, the reflection values of opposite optical vortices are equal as the left-handed tetramer can no longer couple the beams. In contrast, for left-handed tetramers, the reflectance spectrum is exactly inversed compared to right-handed ones (Figure 3c). As a control group, the achiral tetramer shows the same reflection result to left- and right-handed optical vortices (Figure 3b). In the case of chiral trimer (Figure S3) and pentamer (Figure S6), opposite reflectance

https://doi.org/10.1021/acsphotonics.3c00266
ACS Photonics 2023, 10, 1873−1881

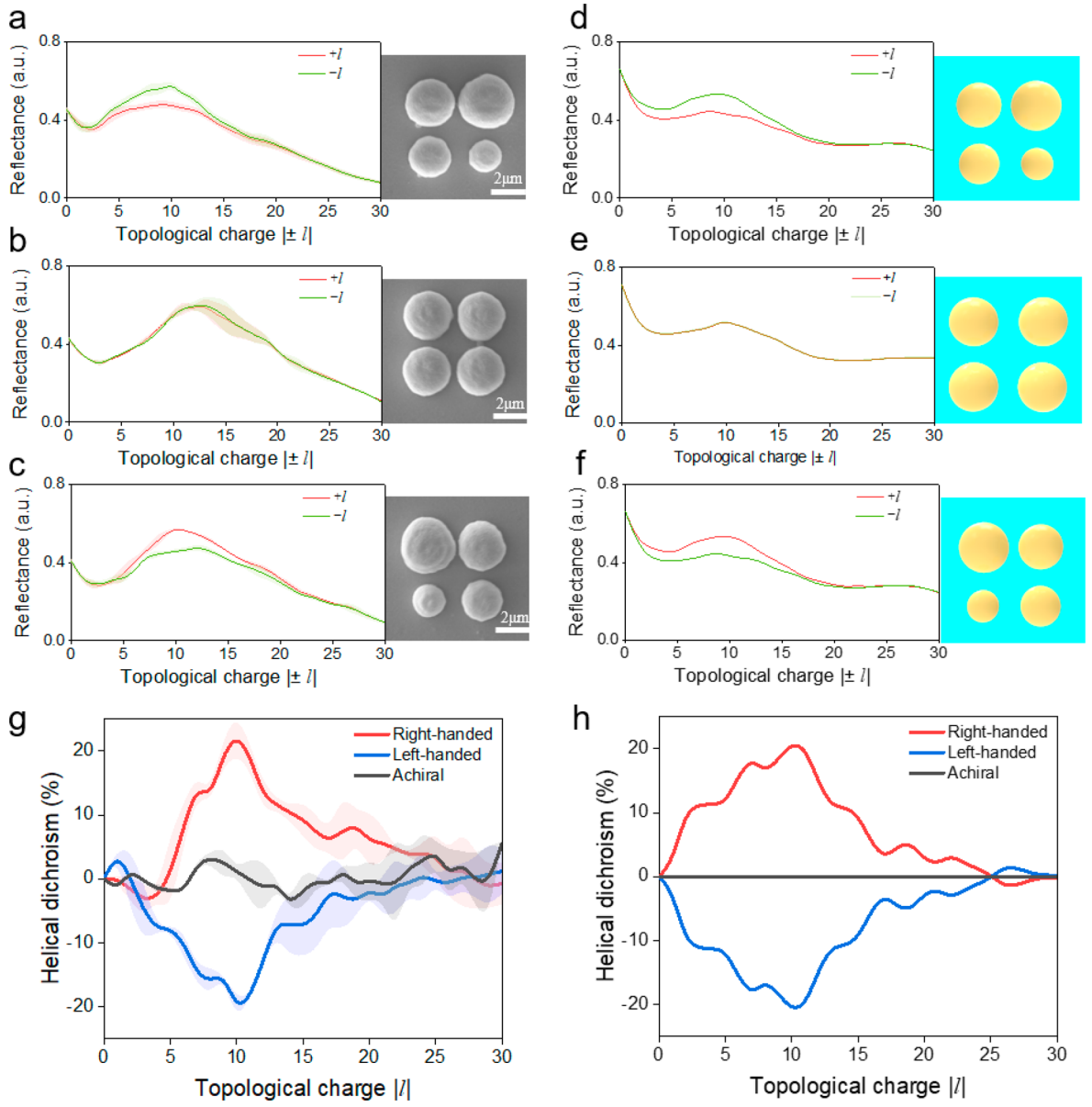

Figure 3. Experimental and simulated reflectance and HD spectra on varying 3D tetramers. Measured reflectance spectra on left-handed (a), right-handed (b), and achiral (c) tetramers by optical vortices with topological charge l from −30 to 30. Solid lines represent the mean value, and shadings represent the standard deviation of multiple measurements. The insets on the right are scanning electron microscope (SEM) images of the corresponding structure. (d−f) Simulated reflectance spectra corresponding to (a)−(c), respectively. (g−h) Measured (g) and simulated (h) HD spectra of three types of tetramers. All the tetramers have identical separation distance d = 600 nm.

spectra are also observed, which proves the universality of HD phenomenon to oligomers.

In order to verify the experimental results, numerical simulations are performed by the commercial finite-difference time-domain (FDTD) method apropos of the three types of tetramers with different configurations (see more details in the Methods section), as shown in Figure 3d−f. The simulation results are in good agreement with the experimental data, indicating that the arrangement of the oligomers can indeed determine the transmission behavior of the OAM beams.

For the sake of quantitatively analyzing HD, we analogized the evaluation index of asymmetric factor in CD response and defined HD of 3D oligomers as

$$\mathrm{HD}_{|l|} = \frac{R_\theta^{+l} - R_\theta^{-l}}{(R_\theta^{+l} + R_\theta^{-l})/2} \times 100\% \quad (1)$$

The HD spectrum showed positive, negative, and approximately zero HD values for right-handed, left-handed, and achiral tetramers in the coupling region ($2 < |l| < 25$), respectively (Figure 3g). According to theory (Supporting Information, section S1), the HD signals of left-handed oligomers and right-handed oligomers should be completely opposite. The slight asymmetry of the measured HD spectrum is due to the incomplete mirror symmetry of the left- and right-handed tetramers in fabrication and the uncertainty in optical measurements. The HD signals of the right- and left-handed tetramers are symmetrically distributed, indicating that the chiral features of oligomers can manipulate the transmission

https://doi.org/10.1021/acsphotonics.3c00266
ACS Photonics 2023, 10, 1873−1881

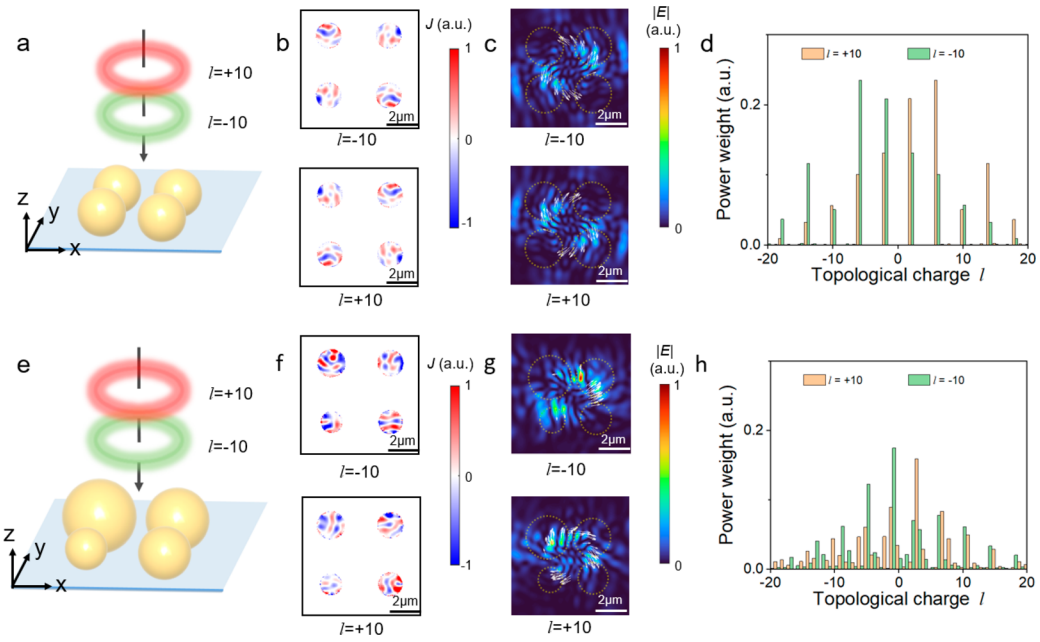

Figure 4. Characterization and origin analysis of helical dichroism of individual 3D tetramers. (a–d) Symmetric surface photocurrent (b), electric field distributions (c), and discrete OAM spectra (d) of $l = -10$ and $l = +10$ on the achiral oligomer (a). (e–h) Corresponding to the right-handed tetramer. White arrows in (c) and (g) indicate the Poynting vectors. The simulated planes of (b) and (f) are located at half height of the minimum ligand at 800 nm above the substrate, so the space between four ligands appears larger than it actually is. The simulated planes of (c) and (e) are located at 2000 nm above the tetramers. Scale bars, 1 μm.

behavior of OAM beams. The HD spectrum of right-handed tetramer peaks at $|l| \approx 10$ and converges to zero after $|l| > 25$. The left-handed tetramer has a spectral line that is approximately mirror-symmetrical to that of the right-handed tetramer. It means that the diameter of optical vortex best matches the size of the tetramers at $|l| \approx 10$, and we can obtain a strongest HD signal (~23%). With the increase of topological charge, the vortex diameter gradually expanded, and the light–matter interaction area also shifted outward. When the topological charge value $|l| > 25$, the HD signal drops to zero since the optical vortex is completely dissociated from the chiral tetramer.

Origin of the HD Phenomenon on 3D Oligomers. HD phenomenon is the outward manifestation of chiral light–matter interaction. To delve into the origin of HD, a series of numerical simulations were employed on achiral (Figure 4a) and right-handed tetramer (Figure 4e), respectively. The physical explanation of HD can be directly observed from the calculated electric current distributions induced by optical vortices with opposite topological charges, as shown in Figure 4b,f. For the achiral tetramers, although the current is twisted under the influence of the optical vortex, this effect is equivalent for an achiral tetramer with C_4 symmetry. Due to the linear polarization of the incident optical vortex, the current distributions demonstrate a 2-fold rotational symmetry, which has no influence on the generation of HD. However, when the symmetry of the structure is broken, there are significantly incoordinate current distribution between optical vortices with topological charge $l = -10$ and +10, which means that the light–matter interactions in the two cases are asymmetric, resulting in the difference in the intensity of reflection.

The electric field distribution (Figure 4c,g) provides a more visual way to observe the physical interpretation of HD. For an achiral tetramer (Figure 4c), the optical vortices with opposite topological charges exhibit perfectly mirrored symmetric distributions. But for the right-handed tetramer (Figure 4g), distinct electric field distributions have been observed at 2000 nm above the tetramer between optical vortices with topological charges $l = +10$ and -10. By observing the relative electric field intensity for $l = -10$ and $l = +10$, it is found that compared with $l = -10$, the reflection intensity of optical vortex with topological charge $l = +10$ is significantly stronger, which is consistent with the measured reflection spectrum. Due to the inherent symmetry of HD, we infer that the left-handed oligomer demonstrates the inversion-symmetric intensity distributions (Figure S2).

From another perspective, the HD phenomenon is the result of the conversion in power weights of the incident optical vortex. Generally, the azimuthal angular electric field distribution $E(\rho,\varphi)$ can be regarded as the composition of countless orthogonal basis with ratio $\psi_l(\rho)$ in the Hilbert space, where ρ is the distance from the center phase singularity, and ρ is the azimuth angle. Therefore, the corresponding OAM spectrum $\psi_l(\rho)$ can be described as

$$\psi_l(\rho) = \frac{1}{\sqrt{2\pi}} \int_{-\pi}^{+\pi} E(\rho, \varphi) e^{-il\varphi} \, d\varphi \tag{2}$$

According to this theory, simulated discrete OAM spectra of achiral and right-handed tetramers can be obtained respectively by importing electric field distribution data into mathematical software MATLAB for further processing (Figure 4d,h). More details can be found in the Supporting Information, section S2. Obviously, for a couple of optical vortices with opposite topological charges $l = -10$ and +10, the discrete OAM spectrum is axially symmetric at zero, indicating that the achiral oligomers interact equally with the two types of optical vortices. On the other hand, due to the differential electric field modulation by the right-handed tetramer, the two

https://doi.org/10.1021/acsphotonics.3c00266
ACS Photonics 2023, 10, 1873–1881

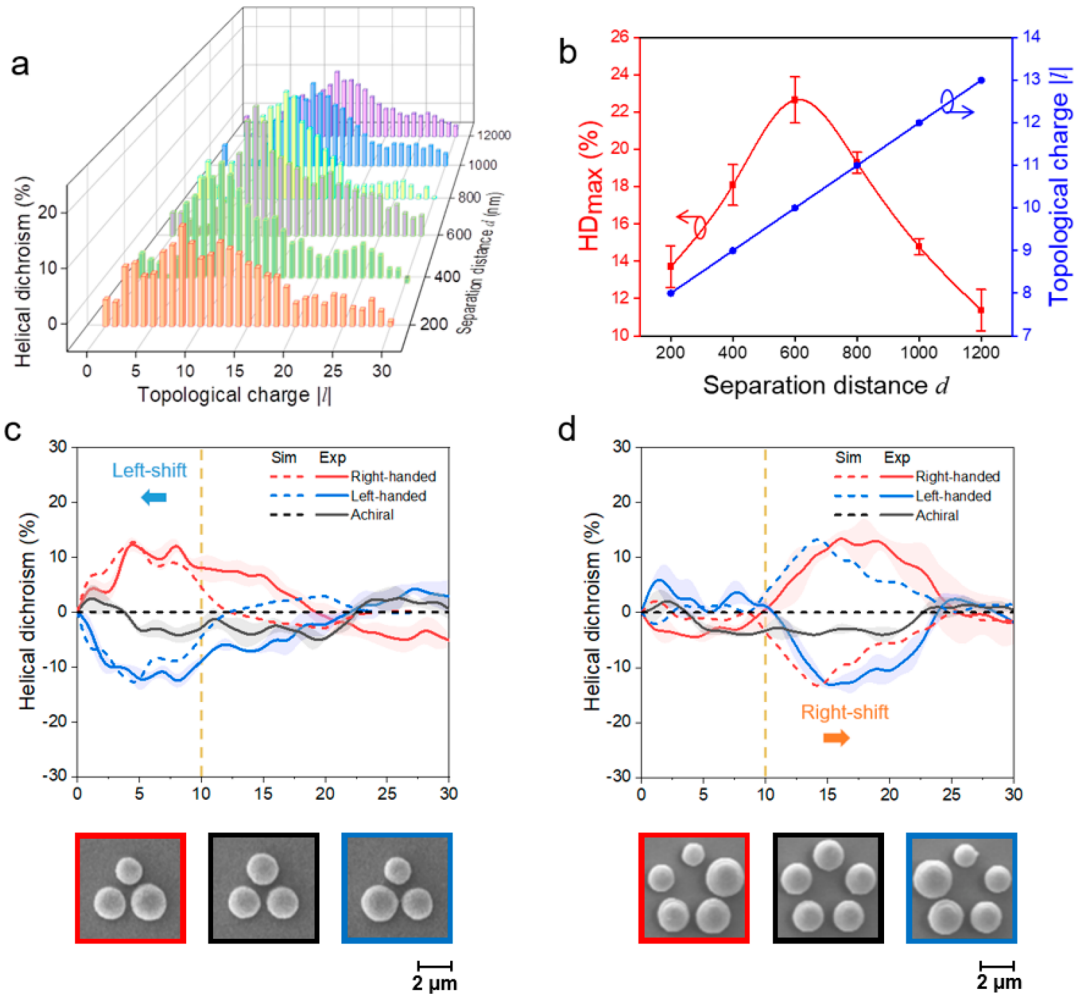

Figure 5. HD spectra of 3D oligomers with varying parameters. (a) HD spectra of the right-handed tetramer with incremental separation distance d ranging from 200 to 1200 nm. (b) Maximum HD values (red dots) and corresponding topological charge $|l|$ (blue dots) for different separation distance d. (c, d) Measured HD spectra on trimer (c) and pentamer (d), respectively. The golden dotted line shows the peak position of HD spectrum of the tetramer. The separation distances are all 600 nm.

sides of the discrete OAM spectrum show great asymmetry, and some power weights appear at the new topological charges. Consequently, the symmetric breaking of discrete OAM spectra can be regard as another explanation for the origin of HD.

Tailoring HD of 3D Oligomers with Varying Parameters. Because of the simple construction of the oligomer, we can easily tailor its HD by tuning the geometric parameters. In particular, multiple oligomers can even be assembled as chiral building blocks for yielding a strong chiroptical response.[49−52] Hence, it is meaningful to analyze the dependence of HD on a specific parameter, in order to design more complex optical metamaterials for optical communication, imaging, and sensing.

The principle of this parameter-tailored experiments is the univariate control method, i.e., independently tuning one parameter while keeping others unchanged. The dependence can be obtained by observing the changes of HD peaks. As shown in Figure 5a, we measured HD spectra of the tetramers with the same configuration but varying separation distance d from 200 to 1200 nm at a step of 200 nm to figure out the spacing dependence of HD of 3D tetramers. The peak position of HD spectrum of tetramer with larger separation distance will shift to a larger topological charge value. In our measurements, the maximum HD signal is obtained when d = 600 nm (Figure 5b). When separation distance d < 600 nm, the maximum peak value increases for larger d. When d > 600 nm, the maximum peak value decreases with the increase of d. As a result, we can easily engineer the HD spectra of chiral oligomers by adjusting d to achieve a robust chiroptical response.

In addition, the impact of another crucial parameter, the ligands number, has also been researched. Figure 5c,d illustrate the experimental HD spectra of the trimers and pentamers. In the premise of the same separation distance, a higher ligands number leads to a larger overall size, and the peak position of HD spectrum right-shifts correspondingly with the increase of the size of 3D oligomers. As a result, compared with the peak position of the tetramer, the peak of the trimer is shifted to the left while the pentamer is shifted to the right. On the other hand, we found that the peaks for trimers and pentamers were only around 13% compared to 23% for tetramers. In contrast to the regular change of the peak position, the peak size does not have a good trend of change, which does not hinder the promotion of the concept of chiral center in the field of optical metamaterials.

https://doi.org/10.1021/acsphotonics.3c00266
ACS Photonics 2023, 10, 1873−1881

CONCLUSIONS

In summary, we have demonstrated the OAM-dependent HD of individual 3D oligomers via optical vortices with varying topological charges. These simple-constructed chiral tetrameric metamaterials can yield a gigantic HD signal up to ∼23%. Moreover, by simulation analysis of electric current distribution, electric field distribution, and the discrete OAM spectroscopy, the origin of the HD phenomenon on the 3D oligomers was revealed. In addition, we engineer the separation distance and the ligands number of the 3D oligomers for obtaining various HD spectra. Based on these results, we expect that individual 3D oligomers can be used as basic building blocks to construct multiple chiral center metamaterials which mimics biological macromolecules. Our work validates the application of bioinspired chiral oligomers for photonic OAM manipulation, providing a novel pattern for the design of complex optical metamaterials.

METHODS

Manufacturing of the 3D Oligomers. The main material for manufacturing 3D oligomers is a commercially available zirconium−silicon hybrid sol−gel (SZ2080, IESLFORTH, Greece). Thanks to its negligible shrinkage, we were able to produce oligomers consistent with the design. Before direct laser writing, it is necessary to perform prebaking process on a thermal platform at 100 °C for 30 min to make sure the solvent in the material has evaporated. The femtosecond laser with a central wavelength of 800 nm is generated by a Ti: Sapphire ultrafine oscillator (Chameleon Vision-S, Coherent, Inc., U.S.) and focuses on the sample through a 60× oil-immersed objective lens (NA = 1.35, Olympus, JPN) for photopolymerization. In order to avoid the influence of the refractive index change of photoresist on the focus position of the beam after polymerization, a top-down scanning strategy was adopted. After that, the polymer material was developed in absolute ethanol for 30 min until all the unpolymerized portion was washed away. At last, we use ion sputter coater (108 AUTO sputter coater, Cressington, U.K.) to deposit ∼10 nm gold on the prefabs.

Experimental Setup for Measurement and Characterization. The phase-only SLM (Pluto NIR-2, Holoeye Photonics AG, GER) has 1920 × 1080 pixels, able to modulate high quality optical vortices. A 100× dry objective lens (NA = 0.9, Olympus, GER) were used in the HD detection. Different types of 3D oligomers are individually aligned with the axes of normal incident optical vortices by a nanoscale 3D piezoelectric platform (E545, Physik Instrumente, U.K.). The reflected intensity was caught by a CCD camera (MV-SUA133GM-T, MindVision, CHN) with the acquisition time of 30 ms. Scanning electron microscopy (SEM) images of the oligomers were acquired by a secondary-electron scanning electron microscope (EVO18, ZEISS, GER).

Numerical Simulation. All the numerical simulations were performed on a commercial finite difference time-domain-based software (FDTD Solutions, Lumerical Solutions, Inc., CAN). In the simulation, the interior refractive index of the 3D oligomers was set to be 1.52 and the refractive index of the outer gold shell referenced the refractive index of gold at wavelength of 800 nm published by Edward Palik. Perfectly matched layer boundaries were employed for the *X*, *Y*, and *Z* direction. The wavelength of the optical vortices was fixed at 800 nm, consistent with the one in the experiment. The electric current distribution and electric field distribution at the location of interest was recorded by a frequency domain power monitor. The commercial mathematical software (MATLAB, MathWorks, U.S.) is used to normalize the simulation results and analyze the data.

ASSOCIATED CONTENT

Supporting Information

The Supporting Information is available free of charge at https://pubs.acs.org/doi/10.1021/acsphotonics.3c00266.

Sections S1 and S2: The generation principle of helical dichroism; Digital spiral spectra of chiral optical fields. Figures S1−S8: Design of 3D tetramers; Electric field distributions of the opposite handedness tetramers; Design of 3D trimers; Experimental and simulated reflectance spectra on varying 3D trimers; Characterization and origin of helical dichroism of individual 3D trimer; Design of 3D pentamers; Experimental and simulated reflectance spectra on varying 3D pentamers; Characterization and origin of helical dichroism of individual 3D pentamer (PDF)

AUTHOR INFORMATION

Corresponding Author

Jiawen Li − *Hefei National Laboratory for Physical Sciences at the Microscale, Key Laboratory of Precision Scientific Instrumentation of Anhui Higher Education Institutes, CAS Key Laboratory of Mechanical Behavior and Design of Materials, Department of Precision Machinery and Precision Instrumentation, University of Science and Technology of China, Hefei 230026, China*; orcid.org/0000-0003-3950-6212; Email: jwl@ustc.edu.cn

Authors

Yang Cao − *Hefei National Laboratory for Physical Sciences at the Microscale, Key Laboratory of Precision Scientific Instrumentation of Anhui Higher Education Institutes, CAS Key Laboratory of Mechanical Behavior and Design of Materials, Department of Precision Machinery and Precision Instrumentation, University of Science and Technology of China, Hefei 230026, China*

Shunli Liu − *Hefei National Laboratory for Physical Sciences at the Microscale, Key Laboratory of Precision Scientific Instrumentation of Anhui Higher Education Institutes, CAS Key Laboratory of Mechanical Behavior and Design of Materials, Department of Precision Machinery and Precision Instrumentation, University of Science and Technology of China, Hefei 230026, China*

Yuan Tao − *Hefei National Laboratory for Physical Sciences at the Microscale, Key Laboratory of Precision Scientific Instrumentation of Anhui Higher Education Institutes, CAS Key Laboratory of Mechanical Behavior and Design of Materials, Department of Precision Machinery and Precision Instrumentation, University of Science and Technology of China, Hefei 230026, China*

Xinghao Wang − *Hefei National Laboratory for Physical Sciences at the Microscale, Key Laboratory of Precision Scientific Instrumentation of Anhui Higher Education Institutes, CAS Key Laboratory of Mechanical Behavior and Design of Materials, Department of Precision Machinery and Precision Instrumentation, University of Science and Technology of China, Hefei 230026, China*

https://doi.org/10.1021/acsphotonics.3c00266
ACS Photonics 2023, 10, 1873−1881

Jincheng Ni − *Hefei National Laboratory for Physical Sciences at the Microscale, Key Laboratory of Precision Scientific Instrumentation of Anhui Higher Education Institutes, CAS Key Laboratory of Mechanical Behavior and Design of Materials, Department of Precision Machinery and Precision Instrumentation, University of Science and Technology of China, Hefei 230026, China*

Chaowei Wang − *Hefei National Laboratory for Physical Sciences at the Microscale, Key Laboratory of Precision Scientific Instrumentation of Anhui Higher Education Institutes, CAS Key Laboratory of Mechanical Behavior and Design of Materials, Department of Precision Machinery and Precision Instrumentation, University of Science and Technology of China, Hefei 230026, China*

Xinyuan Zheng − *Hefei National Laboratory for Physical Sciences at the Microscale, Key Laboratory of Precision Scientific Instrumentation of Anhui Higher Education Institutes, CAS Key Laboratory of Mechanical Behavior and Design of Materials, Department of Precision Machinery and Precision Instrumentation, University of Science and Technology of China, Hefei 230026, China*

Yanlei Hu − *Hefei National Laboratory for Physical Sciences at the Microscale, Key Laboratory of Precision Scientific Instrumentation of Anhui Higher Education Institutes, CAS Key Laboratory of Mechanical Behavior and Design of Materials, Department of Precision Machinery and Precision Instrumentation, University of Science and Technology of China, Hefei 230026, China;* orcid.org/0000-0003-1964-0043

Dong Wu − *Hefei National Laboratory for Physical Sciences at the Microscale, Key Laboratory of Precision Scientific Instrumentation of Anhui Higher Education Institutes, CAS Key Laboratory of Mechanical Behavior and Design of Materials, Department of Precision Machinery and Precision Instrumentation, University of Science and Technology of China, Hefei 230026, China;* orcid.org/0000-0003-0623-1515

Jiaru Chu − *Hefei National Laboratory for Physical Sciences at the Microscale, Key Laboratory of Precision Scientific Instrumentation of Anhui Higher Education Institutes, CAS Key Laboratory of Mechanical Behavior and Design of Materials, Department of Precision Machinery and Precision Instrumentation, University of Science and Technology of China, Hefei 230026, China;* orcid.org/0000-0001-6472-8103

Complete contact information is available at: https://pubs.acs.org/10.1021/acsphotonics.3c00266

Author Contributions

Y.C. and S.L. contributed equally to this work. S.L., Y.C., and J.L. proposed the idea and conceived the experiment. S.L., Y.C., X.W., and Y.T. performed the experiments. S.L., Y.C., and J.N. performed the numerical simulations. Y.C. wrote the manuscript. J.L., S.L., X.Z., Y.H., C.W., J.C., and D.W. reviewed and revised the manuscript.

Funding

This work was supported by the National Natural Science Foundation of China (Nos. 61927814, 52122511, 52075516, 62005262), the National Key Research and Development Program of China (No. 2021YFF0502700), the Major Scientific and Technological Projects in Anhui Province (No.202103a05020005), the USTC Research Funds of the Double First-Class Initiative (YD2340002009), the Open Project of Wuhan National Laboratory for Optoelectronics (No.2019WNLOKF014), CAS Project for Young Scientists in Basic Research (Grant No.YSBR-049), and the Fundamental Research Funds for the Central Universities (WK5290000003).

Notes

The authors declare no competing financial interest.

■ ACKNOWLEDGMENTS

We acknowledge the Experimental Center of Engineering and Material Sciences at USTC for the fabrication and measuring of samples. This work was partly carried out at the USTC Center for Micro and Nanoscale Research and Fabrication.

■ REFERENCES

(1) Bonner, W. A. The origin and amplification of biomolecular chirality. *Origins Life Evol. Biospheres* **1991**, *21* (2), 59−111.

(2) Agranat, I.; Caner, H.; Caldwell, J. Putting chirality to work: the strategy of chiral switches. *Nat. Rev. Drug. Disc.* **2002**, *1* (10), 753−768.

(3) Luisi, P. L. *The Emergence of Life: from Chemical Origins to Synthetic Biology*; Cambridge University Press, 2016.

(4) Diéguez, M.; Claver, C.; Pàmies, O. Recent Progress in Asymmetric Catalysis Using Chiral Carbohydrate-Based Ligands. *Eur. J. Org. Chem.* **2007**, *2007* (28), 4621−4634.

(5) Maruoka, K.; Ooi, T. Enantioselective amino acid synthesis by chiral phase-transfer catalysis. *Chem. Rev.* **2003**, *103* (8), 3013−3028.

(6) Corradini, R.; Sforza, S.; Tedeschi, T.; Marchelli, R. Chirality as a tool in nucleic acid recognition: Principles and relevance in biotechnology and in medicinal chemistry. *Chirality* **2007**, *19* (4), 269−294.

(7) Bruice, P. Y. *Essential Organic Chemistry*; Pearson Education Upper Saddle River, 2006.

(8) Fox, M. A.; Whitesell, J. K. *Organic chemistry*; Jones & Bartlett Learning, 2004.

(9) Chen, W.; Bian, A.; Agarwal, A.; Liu, L.; Shen, H.; Wang, L.; Xu, C.; Kotov, N. A. Nanoparticle superstructures made by polymerase chain reaction: collective interactions of nanoparticles and a new principle for chiral materials. *Nano Lett.* **2009**, *9* (5), 2153−2159.

(10) Hentschel, M.; Schäferling, M.; Weiss, T.; Liu, N.; Giessen, H. Three-dimensional chiral plasmonic oligomers. *Nano Lett.* **2012**, *12* (5), 2542−2547.

(11) Đorđević, L.; Arcudi, F.; D'Urso, A.; Cacioppo, M.; Micali, N.; Bürgi, T.; Purrello, R.; Prato, M. Design principles of chiral carbon nanodots help convey chirality from molecular to nanoscale level. *Nat. Commun.* **2018**, *9* (1), 1−8.

(12) Kuzyk, A.; Schreiber, R.; Fan, Z.; Pardatscher, G.; Roller, E.-M.; Högele, A.; Simmel, F. C.; Govorov, A. O.; Liedl, T. DNA-based self-assembly of chiral plasmonic nanostructures with tailored optical response. *Nature* **2012**, *483* (7389), 311−314.

(13) Hentschel, M.; Wu, L.; Schäferling, M.; Bai, P.; Li, E. P.; Giessen, H. Optical properties of chiral three-dimensional plasmonic oligomers at the onset of charge-transfer plasmons. *ACS Nano* **2012**, *6* (11), 10355−10365.

(14) Hentschel, M.; Saliba, M.; Vogelgesang, R.; Giessen, H.; Alivisatos, A. P.; Liu, N. Transition from isolated to collective modes in plasmonic oligomers. *Nano Lett.* **2010**, *10* (7), 2721−2726.

(15) Zu, S.; Bao, Y.; Fang, Z. Planar plasmonic chiral nanostructures. *Nanoscale* **2016**, *8* (7), 3900−3905.

(16) Ogier, R.; Fang, Y.; Svedendahl, M.; Johansson, P.; Käll, M. Macroscopic layers of chiral plasmonic nanoparticle oligomers from colloidal lithography. *ACS Photonics* **2014**, *1* (10), 1074−1081.

(17) Ni, J.; Hu, Y.; Liu, S.; Lao, Z.; Ji, S.; Pan, D.; Zhang, C.; Xu, B.; Li, J.; Wu, D.; Chu, J. Controllable double-helical microstructures by photonic orbital angular momentum for chiroptical response. *Opt. Lett.* **2021**, *46* (6), 1401−1404.

(18) Mastroianni, A. J.; Claridge, S. A.; Alivisatos, A. P. Pyramidal and chiral groupings of gold nanocrystals assembled using DNA scaffolds. *J. Am. Chem. Soc.* **2009**, *131* (24), 8455−8459.
(19) Hentschel, M.; Schäferling, M.; Metzger, B.; Giessen, H. Plasmonic diastereomers: adding up chiral centers. *Nano Lett.* **2013**, *13* (2), 600−606.
(20) Banzer, P.; Woźniak, P.; Mick, U.; De Leon, I.; Boyd, R. W. Chiral optical response of planar and symmetric nanotrimers enabled by heteromaterial selection. *Nat. Commun.* **2016**, *7* (1), 1−9.
(21) Allen, L.; Beijersbergen, M. W.; Spreeuw, R.; Woerdman, J. Orbital angular momentum of light and the transformation of Laguerre-Gaussian laser modes. *Phys. Rev. A* **1992**, *45* (11), 8185.
(22) Zhang, Z.; Qiao, X.; Midya, B.; Liu, K.; Sun, J.; Wu, T.; Liu, W.; Agarwal, R.; Jornet, J. M.; Longhi, S.; et al. Tunable topological charge vortex microlaser. *Science* **2020**, *368* (6492), 760−763.
(23) Chong, A.; Wan, C.; Chen, J.; Zhan, Q. Generation of spatiotemporal optical vortices with controllable transverse orbital angular momentum. *Nat. Photonics* **2020**, *14* (6), 350−354.
(24) Chen, Y.; Du, W.; Zhang, Q.; Avalos-Ovando, O.; Wu, J.; Xu, Q.-H.; Liu, N.; Okamoto, H.; Govorov, A. O.; Xiong, Q.; Qiu, C.-W. Multidimensional nanoscopic chiroptics. *Nat. Rev. Phys.* **2022**, *4* (2), 113−124.
(25) Ren, H.; Fang, X.; Jang, J.; Bürger, J.; Rho, J.; Maier, S. A. Complex-amplitude metasurface-based orbital angular momentum holography in momentum space. *Nat. Nanotechnol.* **2020**, *15* (11), 948−955.
(26) Fang, X.; Ren, H.; Gu, M. Orbital angular momentum holography for high-security encryption. *Nat. Photonics* **2020**, *14* (2), 102−108.
(27) Djordjevic, I. B. Deep-space and near-Earth optical communications by coded orbital angular momentum (OAM) modulation. *Opt. Express* **2011**, *19* (15), 14277−14289.
(28) Willig, K. I.; Rizzoli, S. O.; Westphal, V.; Jahn, R.; Hell, S. W. STED microscopy reveals that synaptotagmin remains clustered after synaptic vesicle exocytosis. *Nature* **2006**, *440* (7086), 935−939.
(29) Gu, M.; Kang, H.; Li, X. Breaking the diffraction-limited resolution barrier in fiber-optical two-photon fluorescence endoscopy by an azimuthally-polarized beam. *Sci. Rep.* **2014**, *4* (1), 1−6.
(30) Curtis, J. E.; Grier, D. G. Structure of optical vortices. *Phys. Rev. Lett.* **2003**, *90* (13), 133901.
(31) Pan, D.; Liu, S.; Li, J.; Ni, J.; Xin, C.; Ji, S.; Lao, Z.; Zhang, C.; Xu, B.; Li, R.; et al. Rapid Fabrication of 3D Chiral Microstructures by Single Exposure of Interfered Femtosecond Vortex Beams and Capillary-Force-Assisted Self-Assembly. *Adv. Funct. Mater.* **2022**, *32* (4), 2106917.
(32) Ni, J.; Wang, C.; Zhang, C.; Hu, Y.; Yang, L.; Lao, Z.; Xu, B.; Li, J.; Wu, D.; Chu, J. Three-dimensional chiral microstructures fabricated by structured optical vortices in isotropic material. *Light Sci. Appl.* **2017**, *6* (7), e17011.
(33) Liu, S.; Ni, J.; Zhang, C.; Wang, X.; Cao, Y.; Wang, D.; Ji, S.; Pan, D.; Li, R.; Wu, H.; et al. Tailoring Optical Vortical Dichroism with Stereometamaterials. *Laser Photonics Rev.* **2022**, *16* (2), 2100518.
(34) Ni, J.; Liu, S.; Wu, D.; Lao, Z.; Wang, Z.; Huang, K.; Ji, S.; Li, J.; Huang, Z.; Xiong, Q.; et al. Gigantic vortical differential scattering as a monochromatic probe for multiscale chiral structures. *Proc. Natl. Acad. Sci. U. S. A.* **2021**, *118* (2), e2020055118.
(35) Ni, J.; Liu, S.; Hu, G.; Hu, Y.; Lao, Z.; Li, J.; Zhang, Q.; Wu, D.; Dong, S.; Chu, J.; Qiu, C.-W. Giant helical dichroism of single chiral nanostructures with photonic orbital angular momentum. *ACS Nano* **2021**, *15* (2), 2893−2900.
(36) Rouxel, J. R.; Rösner, B.; Karpov, D.; Bacellar, C.; Mancini, G. F.; Zinna, F.; Kinschel, D.; Cannelli, O.; Oppermann, M.; Svetina, C.; et al. Hard X-ray helical dichroism of disordered molecular media. *Nat. Photonics* **2022**, *16*, 570−574.
(37) Kerber, R.; Fitzgerald, J.; Xiao, X.; Oh, S. S.; Maier, S.; Giannini, V.; Reiter, D. Interaction of an Archimedean spiral structure with orbital angular momentum light. *New J. Phys.* **2018**, *20* (9), 095005.
(38) Kerber, R. M.; Fitzgerald, J. M.; Reiter, D. E.; Oh, S. S.; Hess, O. Reading the orbital angular momentum of light using plasmonic nanoantennas. *ACS Photonics* **2017**, *4* (4), 891−896.
(39) Guo, Y.; Zhu, G.; Bian, W.; Dong, B.; Fang, Y. Orbital angular momentum dichroism caused by the interaction of electric and magnetic dipole moments and the geometrical asymmetry of chiral metal nanoparticles. *Phys. Rev. A* **2020**, *102* (3), 033525.
(40) Yue, Z.; Ren, H.; Wei, S.; Lin, J.; Gu, M. Angular-momentum nanometrology in an ultrathin plasmonic topological insulator film. *Nat. Commun.* **2018**, *9* (1), 4413.
(41) Ren, H.; Gu, M. Angular momentum-reversible near-unity bisignate circular dichroism. *Laser Photonics Rev.* **2018**, *12* (5), 1700255.
(42) Ouyang, X.; Xu, Y.; Xian, M.; Feng, Z.; Zhu, L.; Cao, Y.; Lan, S.; Guan, B.-O.; Qiu, C.-W.; Gu, M.; Li, X. Synthetic helical dichroism for six-dimensional optical orbital angular momentum multiplexing. *Nat. Photonics* **2021**, *15* (12), 901−907.
(43) Hendry, E.; Carpy, T.; Johnston, J.; Popland, M.; Mikhaylovskiy, R.; Lapthorn, A.; Kelly, S.; Barron, L.; Gadegaard, N.; Kadodwala, M. Ultrasensitive detection and characterization of biomolecules using superchiral fields. *Nat. Nanotechnol.* **2010**, *5* (11), 783−787.
(44) Abdulrahman, N. A.; Fan, Z.; Tonooka, T.; Kelly, S. M.; Gadegaard, N.; Hendry, E.; Govorov, A. O.; Kadodwala, M. Induced chirality through electromagnetic coupling between chiral molecular layers and plasmonic nanostructures. *Nano Lett.* **2012**, *12* (2), 977−983.
(45) Poynting, J. H. The wave motion of a revolving shaft, and a suggestion as to the angular momentum in a beam of circularly polarised light. *Proc. R. Soc. London, Ser. A* **1909**, *82* (557), 560−567.
(46) Barnett, S. M.; Allen, L. Orbital angular momentum and nonparaxial light beams. *Opt. Commun.* **1994**, *110* (5−6), 670−678.
(47) Yao, A. M.; Padgett, M. J. Orbital angular momentum: origins, behavior and applications. *Adv. Opt. Photon.* **2011**, *3* (2), 161−204.
(48) Yan, W.; Xu, L.; Xu, C.; Ma, W.; Kuang, H.; Wang, L.; Kotov, N. A. Self-assembly of chiral nanoparticle pyramids with strong R/S optical activity. *J. Am. Chem. Soc.* **2012**, *134* (36), 15114−15121.
(49) Wang, M.; Dong, J.; Zhou, C.; Xie, H.; Ni, W.; Wang, S.; Jin, H.; Wang, Q. Reconfigurable plasmonic diastereomers assembled by DNA origami. *ACS Nano* **2019**, *13* (12), 13702−13708.
(50) Decker, M.; Ruther, M.; Kriegler, C.; Zhou, J.; Soukoulis, C.; Linden, S.; Wegener, M. Strong optical activity from twisted-cross photonic metamaterials. *Opt. Lett.* **2009**, *34* (16), 2501−2503.
(51) Zhao, Y.; Belkin, M.; Alù, A. Twisted optical metamaterials for planarized ultrathin broadband circular polarizers. *Nat. Commun.* **2012**, *3* (1), 1−7.
(52) Hentschel, M.; Schäferling, M.; Duan, X.; Giessen, H.; Liu, N. Chiral plasmonics. *Sci. Adv.* **2017**, *3* (5), e1602735.

https://doi.org/10.1021/acsphotonics.3c00266
ACS Photonics 2023, 10, 1873−1881